Evidence for rattling behavior of the filler atom (L) in the filled skutterudites LT_4X_{12} (L=Ce,Eu,Yb; T=Fe,Ru; X=P,Sb) from EXAFS studies

D. Cao,[1,3] F. Bridges,[1] P. Chesler,[1] S. Bushart,[1] E. D. Bauer,[2] and M. B. Maple[2]
[1]*Physics Deparment, University of California, Santa Cruz, California 95064, USA*
[2]*Department of Physics and Institute of Pure and Applied Physical Science, University of California, San Diego, La Jolla, California 92093, USA*
[3]*MS K764, Los Alamos National Laboratory, Los Alamos, New Mexico 87545, USA*
(Received 24 October 2003; revised manuscript received 8 July 2004; published 20 September 2004)

Extended x-ray absorption fine structure (EXAFS) measurements have been carried out at the L K- or L_{III}-edges (L=Ce, Eu, and Yb) and T K-edges (T=Fe and Ru) for a series of filled skutterudite materials, LT_4X_{12} (X=P and Sb). The high correlated Debye temperature ($\Theta_D \sim 400$ K) obtained for the T-X peak indicates that the T_4X_{12} framework is relatively stiff. In contrast, the low Einstein temperature ($\Theta_E \sim 100$ K) obtained for the L-X or T-L pairs strongly supports the concept of a "rattling" local mode behavior for the L ions. The analysis also indicates that this rattling frequency is much smaller in the antimonide skutterudites than in the phosphide ones, and smaller in $CeOs_4Sb_{12}$ than in $CeFe_4Sb_{12}$. Both results indicate that the larger the void within which the Ce atom is located, the lower the rattling frequency. In addition, for some systems in which the signal-to-noise for $\sigma^2(T)$ is high, a fit can be made to extract the reduced mass of the rattling atom; in these cases the obtained reduced mass is close to but slightly below that of the rattler atom mass-clear evidence of a localized mode inside a stiff but not rigid cage. Finally, no clear evidence for any off-center displacement of the filler ions was found in these materials.

DOI: 10.1103/PhysRevB.70.094109 PACS number(s): 61.10.Ht, 63.20.Pw

I. INTRODUCTION

The filled skutterudites, LT_4X_{12} (here L can be a lanthanide, actinide[1] or alkali earth;[2–4] T=Fe, Ru, Os; and X=P, As, Sb) have been studied extensively due to their potential for thermoelectric applications. Transport measurements have shown that these materials have very poor thermal conductivity,[5,6] though most of them are metals (some are even superconductors[7–9]). Such materials meet the phonon glass, electron crystal (PGEC) concept proposed by Slack,[10] who pointed out that a poor thermal conductivity (phonon glass) and good electronic properties (electron crystal) are exactly the properties that a thermoelectric material should have to maximize the thermoelectric figure of merit, $Z=S^2\sigma/\kappa$ (here S is the Seebeck coefficient; σ is the electrical conductivity; κ is the thermal conductivity).

The structure of the binary skutterudites, MX_3, was first identified by Oftedal[11] as space group $Im\bar{3}$. In this structure, 27 transition metal atoms form the framework of one cubic unit cell, which can be subdivided into 8 ($2\times2\times2$) smaller cubic cages. Six of these cubic cages each contains four Sb atoms which form a square ring, while the other two cages are empty. If another type of foreign atom/ion occupies the two remaining void cages, then the filled skutterudite structure is obtained (Fig. 1). (Note that the transition metal atoms in the binary and filled skutterudites are not the same.) Although most of these materials appear metallic (and the absorption edge occurs at the same place as the elemental metal for the framework atoms), the absorption edge for the rattler atom is shifted to the position expected for an ionic configuration; we therefore refer to the rattler as ionic. The "rattler ion" donates electrons to the conduction band which is mainly formed by the hybridization of electronic states from the T and X atoms.

It has been suggested that the rattling of the filler ions in the lattice can effectively scatter phonons and therefore reduce the lattice thermal conductivity. The heat capacity and inelastic neutron scattering studies show that there are low-energy optical vibration modes associated with the filler ions in $La_{0.9}Fe_3CoSb_{12}$ and a few thallium filled antimonide skutterudites.[12,13] However, in order to extract the low-energy optical modes in the filled skutterudites, a comparison of the measurements on different samples was needed for the above mentioned experiments (for example, a comparison

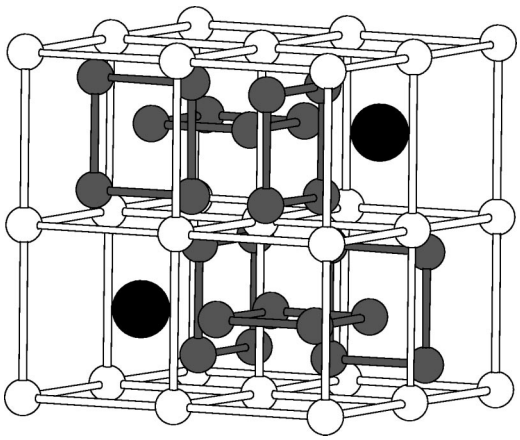

FIG. 1. A sketch of the lattice structure for the filled skutterudites. The white balls are the T atoms which are group VIII transition metal atoms. The gray balls are the X (X=P, As, Sb) atoms and the two black balls with larger size are the lanthanide filler ions. The T atoms form eight small cells in the lattice. Six of them are occupied by square X rings while the other two are occupied by the lanthanide filler ions.

between a binary and a filled skutterudite), and new atoms other than filler ions were introduced into the system during this comparison. The atomic displacement parameter (ADP) results obtained from neutron and x-ray diffraction experiments also show large atomic displacements, U_{iso}, of the filler ions.[14,15] Fitting the temperature dependent U_{iso} to an Einstein model leads to a very low Einstein temperature for the filler ion, which agrees with the "rattling" filler ion concept. Recent extended x-ray absorption fine structure (EXAFS) experiment on a filled skutterudite, $PrOs_4Sb_{12}$, indicate that Pr vibrates with a rather low Einstein temperature ($\Theta_E \sim 75$ K) inside a relatively stiff cage formed by an Os_4Sb_{12} framework.[16] The local density approximation (LDA) calculations of the vibrational density of states also show that La is responsible for the low-energy vibrational modes in $LaFe_4Sb_{12}$.[17]

In this article, we extend our EXAFS results to several other filled skutterudites (Ce, Eu, and Yb filled phosphides or antimonides) and further demonstrate the localized rattling of the filler ions from the local structure point of view. At low *T*, the EXAFS technique can observe the zero point motion for a given atom pair, and the reduced mass of the Einstein oscillator can be determined if the signal-to-noise for $\sigma^2(T)$ is sufficiently high. For a localized mode, the reduced mass should be close to that of the heavy rattling atom, while for other vibrations of the lattice, the reduced mass should be that for the *L*-*X* pair—a much smaller value. For several of the systems discussed here, we indeed find the rattler mass to be close (but slightly smaller) to that of the Ln ion alone, providing evidence for a localized mode of the *L* ion. In addition, the EXAFS analysis also shows that the rattling frequency decreases as the void size increases. As EXAFS can give a rather accurate correlated Debye (or Einstein) temperature for a specific bond (radial motion) without comparison of data for several samples, the EXAFS results reported here provide a reliable and important demonstration of the PGEC concept that is complementary to other measurements.

Experimental details are provided in Sec. II, while Sec. III shows the EXAFS data analysis and discussion. Section IV gives the conclusion.

II. EXPERIMENTAL DETAILS

A. Samples and data collection

Powder samples were used in the EXAFS experiments for all the filled skutterudites. A 400-mesh sieve was used to obtain fine powders after the samples were ground. The fine powders were then brushed onto tape in order to make the EXAFS sample, and the resulting particle size was less than $5-10$ μm. Two pieces of tape were then pressed together (powder-side in) to make a double layer.

EXAFS experiments were carried out on beamline 10-2, 4-2, and 4-3 at SSRL (Stanford Synchrotron Radiation Laboratory) using silicon $\langle 111\rangle$, $\langle 220\rangle$, and $\langle 400\rangle$ monochromator crystals. EXAFS data at the Ce *K*-, Yb L_{III}-, Eu L_{III}-, Fe *K*-, and Ru *K*-edges were taken as a function of temperature. Either a transmission or fluorescence data collection method was used. For transmission collection, the sample was aligned perpendicular to the incoming x-ray beam; for fluorescence collection, samples were aligned 45° with respect to the x-ray beam. In order to create enough absorption, various double layers of sample were used for different edges in the transmission experiments depending on the edge energy (the mean free path increases rapidly with x-ray energy) and the concentration of the absorbing atom. For example, 18 double layers were used when taking Ce *K*-edge (40.4 keV) data while only 1 double layer was used when collecting Fe *K*-edge (7.1 keV) data for $CeFe_4Sb_{12}$.

B. EXAFS technique

In EXAFS, the absorption coefficient, μ, is defined as: $\mu=\mu_0(1+\chi)$. Here μ_0 is the background function (single atom absorption coefficient),[18] and χ is the EXAFS function. $k\chi(k)$ is given by:

$$k\chi(k) = \sum_i k\chi_i(k) = \mathrm{Im}\sum_i A_i \int_0^\infty F_i(k,r)\frac{g_i(r_{0i},r)e^{i(2kr+2\delta_c(k)+\delta_i(k))}}{r^2}dr \quad (1)$$

where χ_i is the EXAFS function for shell *i*, $F_i(k)$ is the backscattering amplitude of the photoelectron from neighbors *i* (it includes mean-free path effects), $g_i(r_{0i},r)$ is the pair distribution function for the atoms at a distance r_{0i}-assumed to be Gaussian for most of this work, and $\delta_c(k)$ and $\delta_i(k)$ are the phase shifts of the central and backscattered photoelectron waves. The amplitude factor A_i is given by

$$A_i = N_i S_0^2, \quad (2)$$

where N_i is the number of equivalent atoms in shell *i*, and S_0^2 is the effective "amplitude reduction factor" that accounts primarily for many-body effects such as shake-up or shake-off, but also includes small corrections to the mean-free path in the theoretical functions. In this equation, the photoelectron wave vector *k* is derived from $k=\sqrt{2m_e(E-E_0)/\hbar^2}$, where E_0 is the binding energy of the *K* or *L* shell electrons of the excited atom.

The Fourier transform (FT) of $k\chi(k)$ (called the *r*-space data) shows peaks that correspond to different atomic shells. However, the position of each peak in the FT plot is shifted from the actual atom-pair distance due to the *k* dependence of the phase shifts $\delta_c(k)$ and $\delta_i(k)$ in Eq. (1). The theoretical standard for each peak in *r*-space data can be calculated using the FEFF7 code (including the phase shift for each peak),[19] according to the crystallographic information obtained from the diffraction experiments. We then fit each peak of interest in the experimental *r*-space data to a theoretical standard with a Gaussian pair distribution function (PDF). In the fit, there are normally four parameters for each peak: σ (width of the PDF), δr (shift of the peak position), *A* (amplitude of the peak), and ΔE_0 (shift of the photoelectron binding energy). Higher cumulants, C_3 and C_4, are also available in the fit but are usually not needed unless the potential is quite anharmonic. For detailed information of

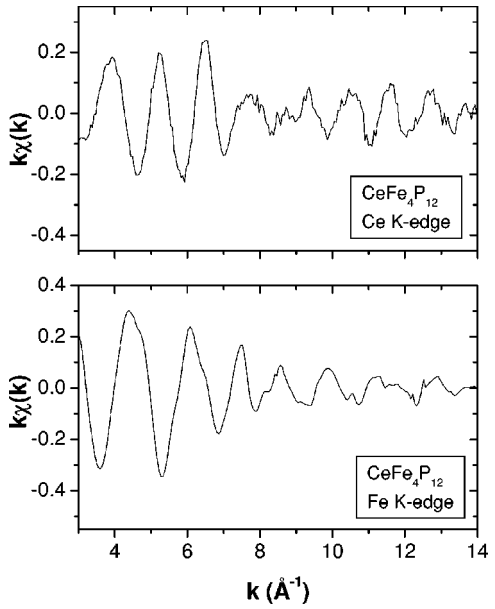

FIG. 2. The Ce *K*- (upper) and Fe *K*-edge (lower) *k*-space data for $CeFe_4P_{12}$ at 20 K.

r-space EXAFS data fits, please see Refs. 20–23.

For a given peak in the *r*-space data, a smaller amplitude at high *T* means a larger width of the PDF; i.e. a larger distortion/disorder of the corresponding atomic shell—it can be static or dynamic. Static distortion/disorder in the lattice (σ_{static}) is from impurities, vacancies, off-center displacements etc., and is *T*-independent (unless there is some transition). Thermal disorder (σ_{thermal}) produced by thermal phonon vibrations is constant at low *T* (zero-point motion), but at high *T*, $\sigma^2_{\text{thermal}}$ is $\propto T$. In many cases one cannot distinguish between random variations of the local distortion from site to site throughout the lattice and a well defined local distortion whose orientation varies throughout the crystal [e.g., a small fixed off-center distortion that splits a peak but cannot be resolved ($\delta_r < 0.1$ Å)]. For larger off-center displacements with larger peak separations ($\delta_r > 0.1$ Å) one can differentiate. Note that small splittings (slightly different bond lengths) that cannot be resolved in EXAFS, are sometimes observed in the diffraction data. Such small distortions, when known, are included in calculating the theoretical EXAFS functions. In much of this paper we will refer to the distortion/disorder as disorder.

III. EXAFS DATA ANALYSIS AND DISCUSSION

Examples of the EXAFS *k*-space data are plotted in Fig. 2 in order to show the quality of the data. The Ce *K*-edge data are a bit noisier than that for the Fe *K*-edge, due in part to the smaller fraction of Ce in the sample. The EXAFS data for other edges (Ru *K*-, Eu L_{III},- and Yb L_{III}-edges) are comparable but the *k*-space plots are not shown.

A. The Ce *K*-edge data

The *r*-space data for the $CeFe_4P_{12}$ and $CeRu_4P_{12}$ samples are shown in Fig. 3; similar data for the three antimonide skutterudites are in Fig. 4. Data at three temperatures, 20, 150, and 300 K, are plotted to show the temperature dependent changes in the local disorder (except for the $CeRu_4Sb_{12}$ sample for which there are only data for the first two temperatures). For the two phosphides, as the temperature increases from 20 to 300 K, the amplitude for the first Ce-P

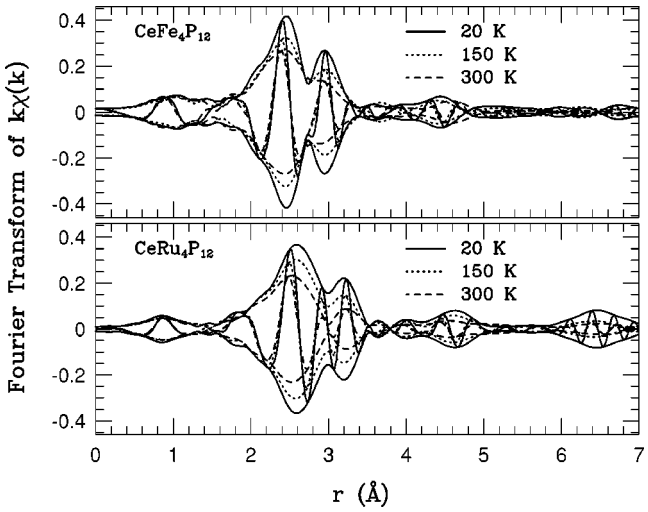

FIG. 3. The *r*-space data (Ce *K*-edge) for $CeFe_4P_{12}$ and $CeRu_4P_{12}$ at three different temperatures. The Fourier transform range is 3.5–13.5 $Å^{-1}$, with 0.3 $Å^{-1}$ Gaussian broadening. The high frequency curve inside the envelope is the real part of the FT (FT_R). The envelope is defined as $\pm\sqrt{FT_R^2+FT_I^2}$, where FT_I is the imaginary part of the FT.

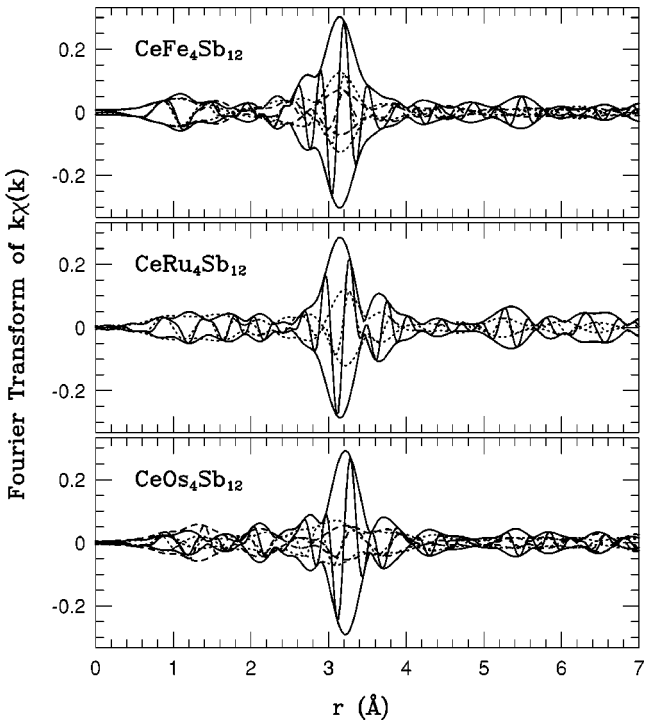

FIG. 4. *r*-space data (Ce *K*-edge) for three Ce filled antimonides at different temperatures (solid line: 20 K; dotted line: 150 K; and dashed line: 300 K). The Fourier transform range is 3.5–13.5 $Å^{-1}$, with 0.3 $Å^{-1}$ Gaussian broadening.

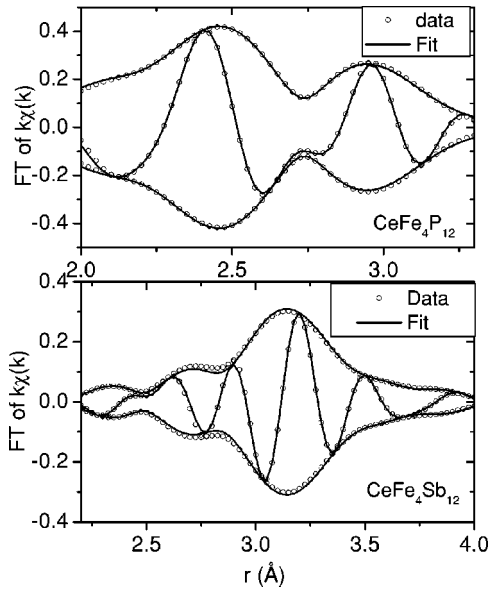

FIG. 5. The fit results of Ce *K*-edge data for $CeFe_4P_{12}$ and $CeFe_4Sb_{12}$ samples at 20 K.

peak (near 2.5 Å) drops ~35% while that for the second peak, Ce-Fe(Ru) (near 3.0 Å for Ce-Fe and 3.2 Å for Ce-Ru) drops ~40%. In contrast for the three antimonides, the change in the amplitude of the first peak (Ce-Sb, near 3.2 Å), is more than 70% over the same temperature range and the amplitude of the second peak for these Sb-samples [Ce-Fe(Ru,Os) near 3.7 Å] is approaching the background noise level at 300 K. This indicates that at room temperature, the local structure of the Ce atoms in the antimonides is much more disordered than in the phosphides. Also note that although the envelope peak moves slightly [a result of the k-dependence of $F_i(k)$ in Eq. (1) and the overlap between peaks] the zero-crossing of FT_R near the center of the first peak in Figs. 3 and 4 does not change; this means that there is very little change in the bond length for the nearest neighbors.

Since we are interested in the rattling behavior of the filler atom (Ce in this case), the main quantity of interest is the peak width, σ. For all samples, fits to the Ce *K*-edge *r*-space data were carried out for the first two atomic shells, Ce-P(Sb) and Ce-Fe(Ru,Os), due to possible interference between the Ce-P(Sb) and Ce-Fe(Ru,Os) peaks. No multiple-scattering peaks occur within the fit range (for phosphides, the fit range is 2–3.3 Å; for antimonides, the fit range is 2.2–4.0 Å). In these fits the amplitudes and ΔE_0 were first determined using the lowest temperature data and then fixed. Four free parameters were used (which is far less than the number of maximum allowed free parameters[24]), to fit the data at each temperature—two σ's and two δr's. For the low T fits, two additional parameters (assumed to be the same for both peaks) were used; S_0^2 and ΔE_0. In all the Ce *K*-edge data fits, S_0^2, obtained from A at low temperatures, was set to be ~0.92. Figure 5 shows several examples of these fits in *r*-space. The extracted σ^2 and atom-pair distances from the fit, for the data at 20 K, are shown in Table I for reference. The obtained atom-pair distances have a very small temperature dependence due to thermal expansion.

TABLE I. The σ^2 and atom-pair distances extracted from the fit for the first two atomic shells (Ce-P(Sb); Ce-Fe(Ru,Os)) at 20 K for the five Ce filled skutterudites. The error bars for the σ^2 and peak distance are 0.0001–0.0003 Å^2 and 0.01–0.02 Å, respectively.

	1st shell: Ce-P(Sb)		2nd shell: Ce-Fe(Ru,Os)	
Sample	σ^2 (Å^2)	Distance (Å)	σ^2 (Å^2)	Distance (Å)
$CeFe_4P_{12}$	0.0021	2.97	0.0033	3.36
$CeRu_4P_{12}$	0.0025	3.09	0.0022	3.45
$CeFe_4Sb_{12}$	0.0034	3.39	0.0047	3.92
$CeRu_4Sb_{12}$	0.0034	3.45	0.0054	4.03
$CeOs_4Sb_{12}$	0.0040	3.47	0.0049	4.00

Figure 6 shows plots of σ^2 vs temperature for each sample. Here the error bars show the relative errors obtained from the variation in σ extracted from fits of several separate scans. There is an overall error in S_0^2 (~10%), which shifts the $\sigma^2(T)$ curve vertically. It is very clear that $\sigma^2(T)$ for the nearest Ce-P or Ce-Sb bond shows a large temperature dependence in each case, and the temperature dependence is much stronger for the three antimonides. Both the neutron diffraction data[14] and our EXAFS data in Sec. III B suggest that the Sb sites in the T_4X_{12} (T=Fe, Ru, Os; X=P, Sb) lattice are well ordered at high T. Thus, this large temperature dependence for the nearest neighbor bonds indicates that it is the Ce site that is highly disordered at high temperature. On the other hand, at low temperature σ^2 is in the range of 0.002–0.004 Å^2, only slightly larger than the value for zero point motion; this shows that there is little static disorder/distortion at low T. Hence, these data show no clear evidence of any Ce off-center displacement for all samples. The large temperature dependence of σ^2 for the Ce-Sb(P) bonds clearly demonstrates the idea of rattling filler atoms in the filled skutterudites.

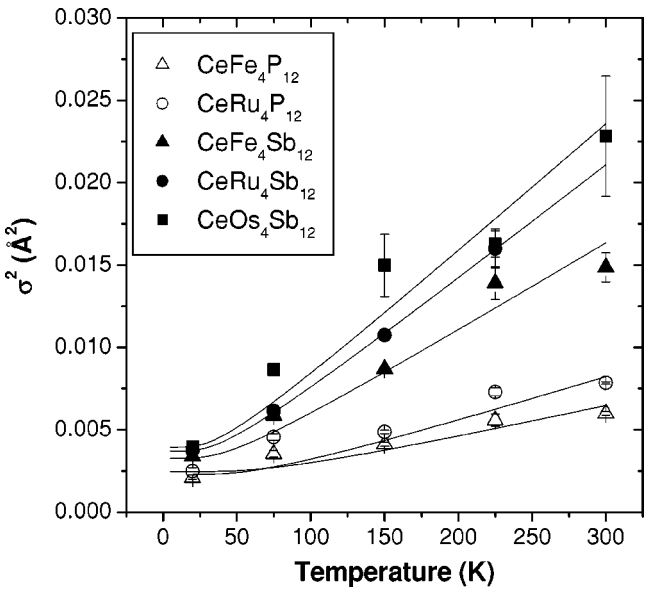

FIG. 6. A plot of σ^2 vs temperature for five Ce filled skutterudites. The solid curves are the fit results to an Einstein model for each sample.

TABLE II. The Einstein temperature of the local vibration as well as the lattice constant and the estimated static disorder for each material. The error for Θ_E and σ^2_{static} are ~5 K and 0.0003–0.0005 Å^2, respectively, for each sample.

Sample	Lattice constant (Å)	Θ_E (K)	σ^2_{static}(Å^2)
$CeFe_4P_{12}$	7.792	148	0.0015
$CeRu_4P_{12}$	8.038	125	0.0012
$CeFe_4Sb_{12}$	9.135	86	0.0018
$CeRu_4Sb_{12}$	9.266	73	0.0010
$CeOs_4Sb_{12}$	9.299	71	0.0020

The phosphide skutterudites have a much smaller unit cell compared with that for the antimonides—the lattice parameter of the antimonides is about 15% larger (see Table II). Including the covalent radii for P (1.06 Å) and Sb (1.38 Å) and the increased lattice constant for antimonide skutterudites, the void in which Ce is located in the antimonides is larger, which can lead to a weaker coupling to the cage atoms, a lower rattling frequency, and hence a larger rattling amplitude. Our EXAFS results strongly support this idea. Since this rattling is a local vibrational mode,[12] it can be described by an Einstein model. Consequently, $\sigma^2_{\text{vib}}(T)$ for the Ce-P(Sb) bond can be written as follows:[25]

$$\sigma^2_{\text{vib}}(T) = \frac{\hbar^2}{2\mu k_B \Theta_E} \coth \frac{\Theta_E}{2T}, \tag{3}$$

and if there is also a static disorder in the sample, we have:

$$\sigma^2_{\text{total}}(T) = \sigma^2_{\text{vib}}(T) + \sigma^2_{\text{static}}. \tag{4}$$

Here μ is the reduced mass of the Einstein vibrator, Θ_E is the Einstein temperature of this vibration mode, T is the temperature, and σ^2_{static} is the static disorder/distortion (temperature independent) in the system. In order to extract detailed information about this local vibrational mode, a fit was carried out for σ^2 vs T using Eqs. (3) and (4). Because of the scatter in the $\sigma^2(T)$ data in Fig. 6, the reduced mass could not be determined with accuracy and good fits could not be obtained without fixing one of the three free parameters (σ^2_{static}, Θ_E and reduced mass μ) in Eqs. (3) and (4). It was assumed that the T_4X_{12} cage (T=Fe, Ru, Os; X=P, Sb) is stiff (consistent with Sec. III B; consequently, the reduced mass, μ, was set equal to the atomic mass for Ce (140 g/mol).

The fit results are shown as solid lines in Fig. 6 for each material and the parameters are given in Table II. The Einstein temperature, Θ_E, clearly decreases (vibration frequency decreases) as the lattice constant increases (larger voids) as shown in Table II. This again confirms the rattling nature of the Ce filler ions.

The LDA calculations suggest that the rattling vibrational modes are essentially harmonic in the filled skutterudites, which then leads to the conclusion that the filler atoms are on center.[26] However, in real materials, whether an atom moves off-center or not depends on a critical balance of local forces. Very small changes on the size of the cage and the radius of the rattler atom can move the atom from an on-center to off-center position.[27,28] Therefore, experiments are needed in order to check the off-center displacement in each system. In fact, an off-center displacement of a similar filler atom was found in other types of thermoelectric materials. For example, a $Eu_8Ga_{16}Ge_{30}$ clathrate sample was shown to have a large Eu off-center displacement (~0.4 Å).[29] Such a large off-center displacement in a material can help scatter phonons[29,30] and lower the thermal conductivity of the material. It is therefore interesting to know if there is any off-center displacement for the filler ions in the filled skutterudites. Note that a static disorder/distortion is needed to fit the σ^2 vs T curve for each sample, but it is very small ($\leqslant$0.002 Å^2). Various defects such as dislocations, interstitials and vacancies could lead to such a static disorder. An off-center displacement of the filler ion would also result in a static distortion in this analysis, but it must be small; an upper limit, assuming no static disorder from any other source in the lattice, is $(\sigma^2_{\text{static}})^{1/2}$, which is about 0.03–0.04 Å. Therefore, there is no clear evidence that the Ce filler ion occupies an off-center position from our EXAFS results.

B. Fe *K*-, Ru *K*-edge data

In order to fully understand the local structure of the filled skutterudites, we also carried out EXAFS experiments at the Fe and Ru *K*-edges for several materials. Examples of the resulting *r*-space data for each edge at various temperatures, are shown in Fig. 7 for $CeFe_4Sb_{12}$ and $CeRu_4Sb_{12}$, respectively. Since Os L_{III}-edge EXAFS data have recently been discussed in Ref. 16 for $PrOs_4Sb_{12}$ we will use those results for comparisons (the results for other Os compounds are similar). In that paper, the analysis of the $\sigma^2(T)$ data yielded a correlated Debye temperature Θ_D~375 K (for the Os-Sb pair).

The first peak in these *r*-space data (near 2.4 Å in Fig. 7) corresponds to the nearest Fe(Ru)-Sb bond. The amplitude of the first peak only drops about 25% as the temperature increases from 20 to 300 K, which indicates moderately stiff bonds. This is a much weaker *T*-dependence when compared to the corresponding ~75% change of the Ce-Sb peak amplitude in Fig. 4, and indicates that neither the Fe(Ru) nor the Sb site is very disordered. The peak near 4.2 Å corresponds to a mixture of the Fe-Fe and Fe-Sb (or Ru-Ru and Ru-Sb) atom pairs.

Fits were carried out on the *r*-space data of the Fe and Ru *K*-edges; S_0^2 was set to be 0.67 and 0.77, respectively. The fit range was from 1.6 to 4.4 Å (Δr=2.8 Å), which includes four peaks: the nearest Fe(Ru)-Sb, Fe(Ru)-Ce, Fe(Ru)-Fe(Ru), and the second nearest Fe(Ru)-Sb peaks. Since the Fourier transform range is 3.5–13.5 Å^{-1} (Δk=10 Å^{-1}), then the maximum number of free parameters we can use in the fit procedure is 19.[24] The amplitude A (which gives S_0^2) and ΔE_0 of each peak were first determined by fitting the lowest temperature data and were then fixed for all other temperatures (in the fits, S_0^2 and ΔE_0 are set to be the same for all peaks). Therefore the total number of free parameters was 8, much less than the allowed number of free parameters. Figure 8 shows an example of the fit quality for the Fe(Ru) *K*-edge

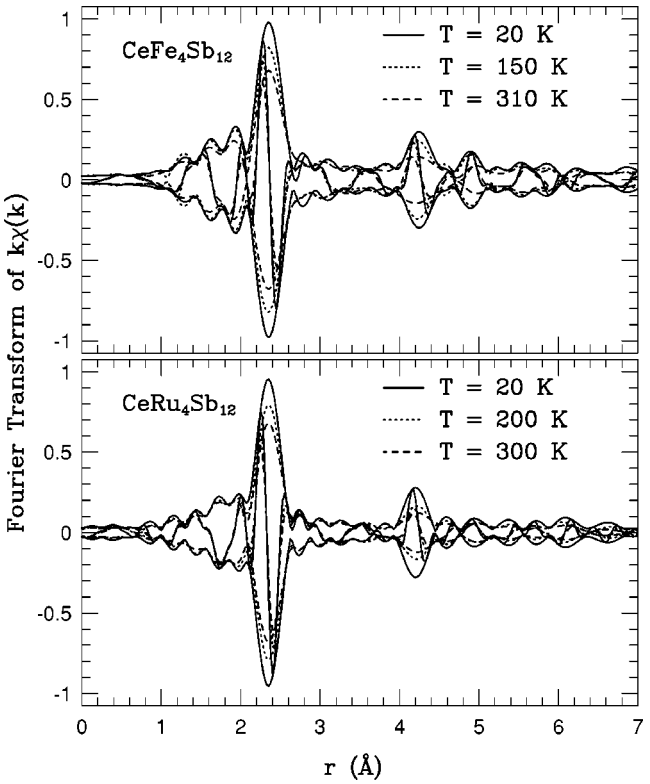

FIG. 7. The *r*-space data of Fe and Ru *K*-edges for $CeFe_4Sb_{12}$ and $CeRu_4Sb_{12}$ in the upper and lower panels, respectively, at three different temperatures to show the temperature dependence. The Fourier transform range is 3.5–13.5 $Å^{-1}$, with a 0.3 $Å^{-1}$ Gaussian broadening.

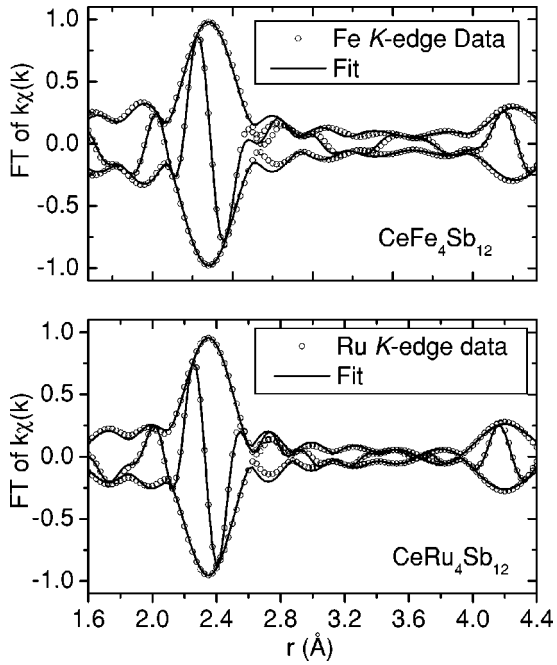

FIG. 8. A plot of the fit results for the Fe and Ru *K*-edge data for $CeFe_4Sb_{12}$ and $CeRu_4Sb_{12}$ at 20 K.

data for $CeFe(Ru)_4Sb_{12}$ at 20 K. Overall, the fit is very good except for the high-*r* part of the first peak near 2.8 Å which is possibly due to a deviation of the theoretical calculation caused by the interstitial scattering outside the muffin-tin radius.[31] Table III shows the σ^2 and distances of different atomic shells obtained from the fit for the data at 20 K.

The resulting values of σ^2 for the first peak (Fe(Ru)-Sb) in the *r*-space data are given in Fig. 9. In order to obtain quantitative values of the stiffness of each bond, we fit σ^2 for each bond to a correlated Debye model and extracted the corresponding Θ_D for the Fe(Ru)-Sb bonds. The fit results are also shown in Fig. 9 as solid and dashed lines for each bond; the values for Θ_D for the Fe-Sb and Ru-Sb bonds are 390 K and 365 K (error: $\sim\pm35$ K), respectively. These results are very similar to Θ_D for the Os-Sb bond ($\sim$375 K) for $PrOs_4Sb_{12}$,[16] but are much larger than the values of Θ_E for the Ce-Sb bond in these materials. Consequently, such results again confirm the idea of an essentially stiff T_4X_{12} framework in the filled skutterudites. Information about the Fe(Ru)-Ce bond [theoretical calculations show that the Fe(Ru)-Ce peaks are at $\sim$3.7 Å in Fig. 7] was also extracted from the fits. However, this peak is very small and not clearly visible in the data [due to the fact that there are only two Ce atoms in each unit cell, and this tiny peak also partially overlaps the Fe(Ru)-Fe(Ru) and the second Fe(Ru)-Sb peaks]. Consequently, we cannot obtain precise broadening information about this peak—although $\sigma^2(T)$ extracted from such fits increases rapidly with *T*, the error bar for each data point is also quite large.

We have also investigated the stiffness of the T_4P_{12} framework for the smaller phosphide skutterudites. The Ru *K*-edge results for $CeRu_4P_{12}$ at several temperatures are shown in the upper panel of Fig. 10 as an example. The first peak (near

TABLE III. The σ^2 and atom-pair distances extracted from the fit with four atomic shells (Fe(Ru)-P(Sb); Fe(Ru)-Ce; second Fe(Ru)-P(Sb); Fe(Ru)-Fe(Ru)) at 20 K for $CeFe_4Sb_{12}$, $CeRu_4Sb_{12}$, and $CeRu_4P_{12}$ samples. In fact, the second Fe(Ru)-P(Sb) peak contains two Fe(Ru)-P(Sb) atom pairs which were combined in our fit due to the close peak distances. The error bars for the σ^2 and peak distance are 0.0001–0.0005 $Å^2$ and 0.01–0.02 Å, respectively.

	1st shell: Fe(Ru)-P(Sb)		2nd shell: Fe(Ru)-Ce		3rd shell: second Fe(Ru)-P(Sb)		4th shell: Fe(Ru)-Fe(Ru)	
Sample	σ^2 ($Å^2$)	Distance (Å)	σ^2 ($Å^2$)	Distance (Å)	σ^2 ($Å^2$)	Distance (Å)	σ^2 ($Å^2$)	Distance (Å)
$CeFe_4Sb_{12}$	0.0007	2.54	0.0043	3.87	0.0060	4.44	0.0065	4.69
$CeRu_4Sb_{12}$	0.0007	2.60	0.0041	4.00	0.0033	4.49	0.0056	4.61
$CeRu_4P_{12}$	0.0018	2.34	0.0025	3.47	0.0050	3.85	0.0025	4.04

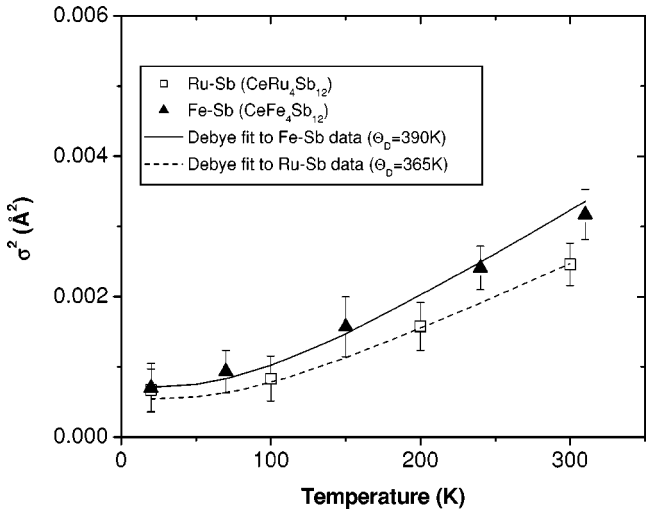

FIG. 9. A plot of σ^2 vs temperature for the Fe(Ru)-Sb peak in Fig. 7. The solid and dashed lines are the Debye-fit results for the Fe-Sb and Ru-Sb bonds, respectively.

1.9 Å) corresponds to the nearest Ru-P bond, and its amplitude only drops ~10% as the temperature increases from 20 K to 300 K. This clearly indicates that the Ru-P bond in $CeRu_4P_{12}$ is quite stiff, which corresponds to a stiff Ru_4P_{12} framework. The Ru-Ce peak is near 3.2 Å which partially overlaps the second nearest Ru-P peak (near 3.4 Å). The Ru-Ru peak is near 3.7 Å. A fit to the Ru *K*-edge *r*-space data was carried out using the procedures described earlier,

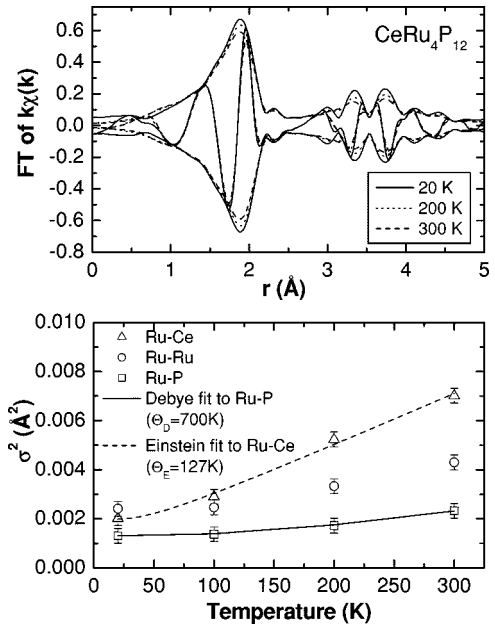

FIG. 10. Upper panel: Ru *K*-edge *r*-space data for $CeRu_4P_{12}$ at three temperatures (20 K, 200 K, and 300 K). Lower panel: Extracted σ^2 as a function of temperature for various atom pairs in $CeRu_4P_{12}$. σ^2 data for Ru-P bond were fit to a Debye model with a Debye temperature of 700 K, while σ^2 data for Ru-Ce pair were fit to an Einstein model with an Einstein temperature of 127 K. The solid line and the dashed line are the results for these two fits, respectively.

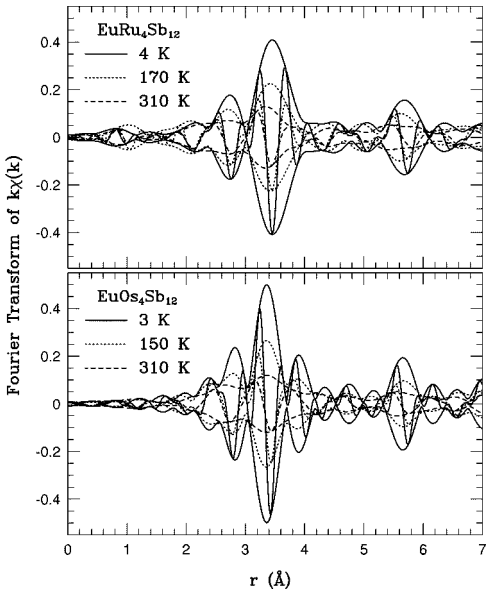

FIG. 11. A plot of the Eu L_{III}-edge *r*-space data for $EuRu_4Sb_{12}$ and $EuOs_4Sb_{12}$ at different temperatures. The Fourier transform range is from 3.5 to 10.3 Å, with a 0.3 Å Gaussian broadening.

for a fit range from 1.2 Å to 3.9 Å. The extracted σ^2 as a function of temperature is shown in the lower panel of Fig. 10 for various atom pairs (see Table III for other parameters obtained from the fit of the data at 20 K). The weak temperature dependence of σ^2 for the nearest Ru-P bond again confirms the stiffness of this bond. A Debye fit to the σ^2 data of Ru-P yields $\Theta_D \sim 700$ K (error: $\sim \pm 70$ K). $\sigma^2(T)$ for the Ru-Ru pair also has a small temperature dependence, in agreement with a stiff Ru_4P_{12} framework. A rather large temperature dependence of σ^2 for the Ru-Ce pair is shown in Fig. 10, which is expected, due to the fact that the Ce-P bond is quite soft for this material (see Sec. III A). An Einstein model was used to fit the $\sigma^2(T)$ data for the Ru-Ce pair (the Ce atomic mass, 140 g/mol, was used as the reduced mass of this vibration, since this is a localized vibration) and an Einstein temperature of 127(5) K was extracted from the fit. This agrees very well with Θ_E for the Ce-P bond, ~125 K, which also provides a consistency check on the Ce-P results.

C. The Eu L_{III}- and Yb L_{III}-edge data

In addition to the experiments on the Ce filler ion, studies of the local structure around other types of filler ions, such as Eu and Yb, were also carried out. All EXAFS experiments on these two types of filler ions were done on the L_{III}-edge using fluorescence collection mode except for the Eu L_{III}-edge data of $EuRu_4Sb_{12}$ which were collected using the transmission mode. The *r*-space data of the Eu L_{III}-edge for $EuRu_4Sb_{12}$ and $EuOs_4Sb_{12}$ are presented in Fig. 11. The Eu-Sb peak is near 3.4 Å in Fig. 11 for both panels (Note: it looks like a double peak because of structure in the backscattering amplitude, and ranges from 2.4 to 3.6 Å), the Eu-Os or Eu-Ru peaks occur near 3.8–3.9 Å and partially overlap the first peak. Both sets of data clearly show a large temperature dependence of the amplitude for the the Eu-Sb

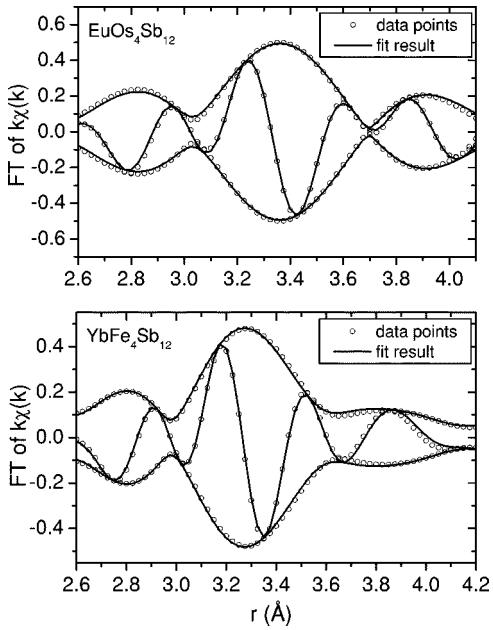

FIG. 12. The fit results for the *r*-space data at Eu L_{III}- and Yb L_{III}-edges for $EuOs_4Sb_{12}$ (at 3 K) and $YbFe_4Sb_{12}$ (at 5 K), respectively.

peak, which is similar to that for the Ce *K*-edge EXAFS (see Sec. III A) and the Pr L_{III}-edge EXAFS for $PrOs_4Sb_{12}$.[16]

A double-peak fit was carried out for the Eu-Sb peak in each set of data in Fig. 11. The fitting procedures were similar to the fits for the Ce *K*-edge data with only δr and σ allowed to vary with *T* for each peak. A fit result to the $EuOs_4Sb_{12}$ data (the fit range is 2.6–4.1 Å) at 3 K is shown in the upper panel of Fig. 12 as an example to show the fit quality. Table IV shows the extracted σ^2 and atom-pair distances from fitting the low temperature data. Figure 13 shows σ^2 vs *T* curves for the Eu-Sb bond, extracted from the Eu L_{III}-edge data of $EuRu_4Sb_{12}$ and $EuOs_4Sb_{12}$. Since the Fe *K*-edge is only ~150 eV above the Eu L_{III}-edge, we could not collect Eu L_{III}-edge EXAFS data for $EuFe_4Sb_{12}$. In these fits $S_0^2=0.94$ for both sets of data. Note that the two plots in Fig. 13 overlap quite well, which suggests that the local structure around the Eu filler ions is essentially the same in these two materials. Detailed fit results given in the first part of Table V also show very similar static disorder/distortion

TABLE IV. The σ^2 and atom-pair distances extracted from the fit for the first two atomic shells (Eu(Yb)-Sb; Eu(Yb)-Fe(Ru,Os)) at the lowest temperature for the three Eu/Yb filled antimonides (4 K for $EuRu_4Sb_{12}$; 3 K for $EuOs_4Sb_{12}$; 5 K for $YbFe_4Sb_{12}$). The error bars for the σ^2 and peak distance are 0.0001–0.0003 $Å^2$ and 0.01–0.02 Å, respectively.

	1st shell: Eu(Yb)-Sb		2nd shell: Eu(Yb)-Fe(Ru,Os)	
Sample	σ^2 ($Å^2$)	Distance (Å)	σ^2 ($Å^2$)	Distance (Å)
$EuRu_4Sb_{12}$	0.0040	3.50	0.0055	4.00
$EuOs_4Sb_{12}$	0.0034	3.50	0.0029	4.07
$YbFe_4Sb_{12}$	0.0037	3.40	0.0034	3.94

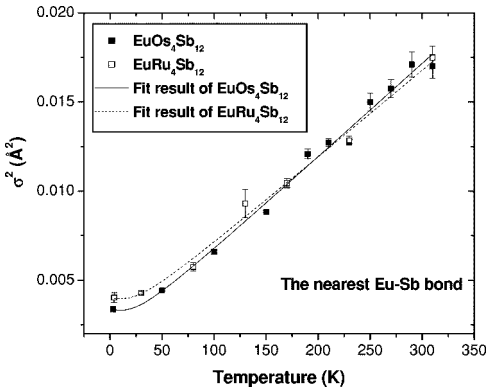

FIG. 13. σ^2 vs temperature for the nearest neighbor Eu-Sb bond in $EuRu_4Sb_{12}$ and $EuOs_4Sb_{12}$. The solid and dashed lines are the fit results to the σ^2 curves for $EuOs_4Sb_{12}$ and $EuRu_4Sb_{12}$, respectively, based on Eqs. (3) and (4).

and Einstein temperatures for them. Since the Eu filler ion is expected to be a local oscillator, the reduced mass μ was first set at 152 g/mol (the atomic mass for the Eu element) in the fit. The Einstein temperatures, Θ_E, for these fits are about ~80 K, which is very similar to that for the Ce *K*-edge data. Since there are more data points and smaller relative error bars for the Eu data, another fit was carried out in which the reduced mass was allowed to vary. Since Θ_E and μ are highly correlated parameters in the fit, large errors were given if both parameters vary simultaneously. Thus we let the fit program determine the best μ for each set of data and then fixed the value of μ to minimize the errors for Θ_E and σ^2_{static}. The resulting reduced mass, shown in the second part of Table V is consistently a little smaller than the corresponding rattler atomic mass, but much larger than the calculated reduced mass (~68) for the Eu-Sb pair. This result strongly confirms the localized nature of the Eu atomic vibrations.

The upper panel of Fig. 14 shows the Yb L_{III}-edge *r*-space data at three different temperatures. The amplitude of the

TABLE V. The fit results for σ^2 vs *T* for the nearest neighbor peak in Eu L_{III}- and Yb L_{III}-edge data for various materials. In the first part, the reduced mass in each fit was set to be the filler ion atomic mass. In the second part, the reduced mass was determined from the fit (estimated error ~40 g/mol) and then fixed to minimize the errors for Θ_E and σ^2_{static}. The errors for Θ_E and σ^2_{static} in the constrained fits are ~5 K and 0.0001–0.0003 $Å^2$, respectively, for each sample.

Sample	μ (g/mol)	Θ_E (K)	σ^2_{static} ($Å^2$)
$EuRu_4Sb_{12}$	152	81	0.0019
$EuOs_4Sb_{12}$	152	78	0.0013
$YbFe_4Sb_{12}$	173	72	0.0017
$EuRu_4Sb_{12}$	133	86	0.0019
$EuOs_4Sb_{12}$	133	82	0.0012
$YbFe_4Sb_{12}$	137	79	0.0014

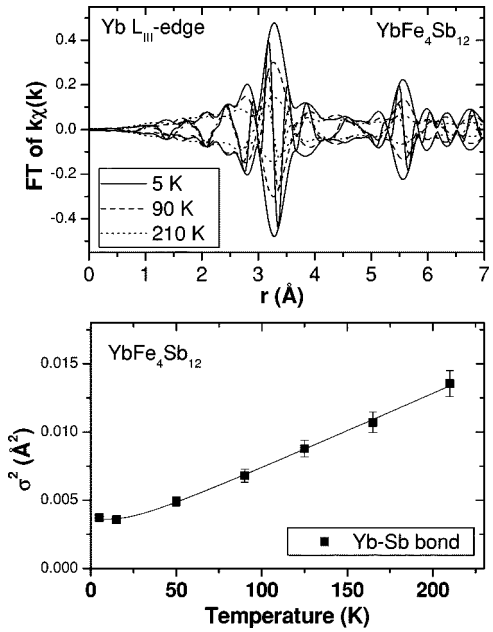

FIG. 14. Upper panel: the Yb L_{III}-edge *r*-space data for $YbFe_4Sb_{12}$ at 20, 90, and 210 K. Lower panel: σ^2 for the Yb-Sb bond as a function of temperature for this material. The solid lines is the Einstein fit, based on Eqs. (3) and (4).

Yb-Sb peak (near 3.3 Å) again shows a very large decrease as temperature increases from 20 to 210 K. Yb L_{III}-edge data at higher temperatures were not collected for this sample. However, the available data set is sufficient to determine the temperature dependence of the first peak in the Yb L_{III}-edge data. Using the fit procedure mentioned earlier in this paper, σ^2 for the Yb-Sb bond as a function of temperature was extracted and is plotted in the lower panel of Fig. 14 (please find other parameters obtained from the fit of the low temperature data in Table IV). The lower panel of Fig. 12 plots an example of the fit to show the fit quality (the fit range is 2.6–4.2 Å). σ^2 for the nearest neighbor Yb-Sb bond in $YbFe_4Sb_{12}$ increases very fast with temperature. The $\sigma^2(T)$ data in this figure were again fit to Eqs. (3) and (4) assuming initially that the reduced mass is equal to the atomic mass of Yb (173 g/mol). The extracted parameters σ^2_{static} and Θ_E are presented in the first part of Table V. A low Einstein temperature, comparable to that for Eu and Ce, is obtained. Relaxing the constraint of a fixed reduced mass leads to a smaller reduced mass (137 g/mol; see the second part of Table V) but still much larger than the reduced mass of the Yb-Sb pair (~72 g/mol).

A similar analysis, in which μ was allowed to vary, was also carried out for σ^2 of the Ru-Ce atom pair in $CeRu_4P_{12}$. A reduced mass of 136 g/mol, which is very close to the Ce atomic mass (140 g/mol), was extracted from the fit. This indicates that Ce "rattling" in $CeRu_4P_{12}$ is an even more localized vibration, which is expected since the Ru_4P_{12} framework is much stiffer than the antimonides (Θ_D for Ru-P is ~700 K).

An upper limit for a possible Pr off-center displacement was reported in Ref. 16, where a slightly larger static disorder/distortion was observed ($\sigma^2_{\text{static}} \sim 0.0045$ Å^2). In Table V, we find that the three materials studied here have reasonably small σ^2_{static} for the Eu(Yb)-Sb bonds, which is similar to that of the Ce-Sb(P) bonds described earlier. Therefore, no clear evidence of a Eu or Yb off-center displacement was found in these materials. The maximum value of a possible off-center displacement, $(\sigma^2_{\text{static}})^{1/2}$, is about ~0.03–0.04 Å for Eu and Yb filler ions.

D. Discussion

The above results show that for the filled antimonide skutterudites, the Einstein temperatures for different rattlers are quite similar; Θ_E varies from ~70 to 90 K depending on the rattler atom and whether or not one assumes the reduced mass to be that of the rattler mass. The reduced mass μ should be somewhat less than the rattler mass if there is some coupling to the surrounding cage; this was observed in cases where the signal-to-noise was sufficiently high.

At present, there are few equivalent measurements available in the literature with which to compare. Sales *et al.*[32] obtain $\Theta_E = 79$ K for La in $LaFe_4Sb_{12}$, from the temperature dependence of the ADP parameter in diffraction for $LaFe_4Sb_{12}$, while Keppens *et al.*[12] obtain 70 K for $La_{0.9}Fe_3CoSb_{12}$, both in good agreement with our results. For Tl in $Tl_{0.22}Co_4Sb_{12}$ Sales *et al.*[15] obtain a slightly lower value: 52 K; while a 57 K Θ_E was also found in some other Tl filled skutterudites.[13] We have observed a small decrease in Θ_E as the void size increases. It would be useful to have additional measurements using other probes to check this in more detail.

For the phosphide skutterudites, the Einstein temperature is significantly larger, $\Theta_E = 125$ and 148 K for $CeRu_4P_{12}$ and $CeFe_4P_{12}$ respectively; this is likely the combined result of a stiffer cage and a smaller void size. Estimates based on calculated force constants (and the rattler mass) for other phosphide systems are[33] 115 K (82 cm^{-1}) for $TlFe_4P_{12}$ and 200 K (141 cm^{-1}) for $LaFe_4P_{12}$. These results are roughly comparable to our results, but EXAFS measurements on the same compounds are needed to provide a better comparison.

We also have determined the correlated Debye temperature—this preferentially probes the strength of the nearest neighbor bond (e.g., Fe-Sb) and, thus, will correspond closer to the longitudinal modes. Measurements of Θ_D from the speed of sound or the low *T* specific heat will generally be smaller since they average over longitudinal and transverse modes, and might include rattler mode contributions. For several of the binary Sb-skutterudites, estimates for Θ_D are near 300 K,[32,34,35] in reasonable agreement with our higher values in view of the differences in the quantities measured. The Mössbauer experiment on $CeFe_4Sb_{12}$ shows a ~450 K Mössbauer lattice temperature[36] which agrees quite well (within the errors) with the 390 K Θ_D for Fe-Sb bond obtained from our XAFS experiments. However, estimates of Θ_D for several Yb-filled compounds (from the specific heat) are considerably lower—190–230 K.[37,38] This is surprising as the lattice constant changes by only a small amount when rattler atoms are incorporated. However, the rattler mode should also contribute to the low temperature specific heat. This will increase the slope of the $C(T)/T$ vs T^2 plot, which

would lead to a lower Θ_D; additional measurements are needed to check this aspect.

Finally there are very few estimates of Θ_D for the phosphide skutterudites. Our value of the correlated Debye temperature (700 K) for $CeRu_4P_{12}$ is much larger than that obtained using low temperature specific heat data.[39] Again, this difference is probably due to the fact that the low-T specific heat is an average of transverse and longitudinal modes plus a contribution at low T from the Ce rattler. EXAFS is most sensitive (for the first neighbors) to radial displacements, i.e., longitudinal modes.

IV. CONCLUSIONS

The EXAFS results clearly show that the filler ions in the filled skutterudites are rattling inside an over-sized cage with very low frequencies ($\Theta_E \sim 80$ K). For the series of Ce filled skutterudites, the rattling frequency decreases as the lattice constant of the sample increases. The Einstein temperature of the filler ion rattling varies from 71 to 86 K for the reported antimonide skutterudites, while it is clearly larger for the phosphide skutterudites with Θ_E ranging from 125 to 148 K.

The T_4X_{12} framework is essentially stiff compared to the thermally disordered filler ion sites at 300 K. Since the filler ions can rattle around without significantly distorting the neighboring atoms in the framework, this strongly supports the idea of a localized vibration for the filler ions in the filled skutterudites, which, therefore, demonstrates the PGEC concept directly from the local structure point of view.

The large reduced mass extracted for Eu-Sb, Yb-Sb, and Ru-Ce atom pairs provides further demonstration of a localized vibration of the filler ion, though our analysis indicates that a small interaction still occurs between the filler ion and the rest of that lattice.

Most materials discussed in this paper have a very small local static disorder/distortion, σ^2_{static}, of the nearest Ln-Sb bond (σ^2_{static} is about $0.001-0.002$ Å^2). Considering the Ln-Sb bond distance is ~ 3.9 Å, this level of static disorder is not unusual. Although in some other thermoelectric materials, such as $Eu_8Ga_{16}Ge_{30}$, the filler atom is off-center[29] (~ 0.4 Å), there is no indication that the filled skutterudites reported in this paper have any off-center filler ions. The maximum value of any off-center displacement for the filler ions in these materials is estimated to be $0.03-0.04$ Å.

ACKNOWLEDGMENTS

The work at UCSC was supported by NSF Grant No. DMR0071863; the work at UCSD was supported by the Department of Energy, under Grant No. DE FG03-86ER-45230, and under the NEDO International Joint Research Program. The experiments were performed at SSRL, which is operated by the DOE, Division of Chemical Sciences, and by the NIH, Biomedical Resource Technology Program, Division of Research Resources.

[1] D. J. Braun and W. Jeitschko, J. Less-Common Met. **76**, 33 (1980).
[2] N. T. Stetson, S. M. Kauzlarich, and H. Hope, J. Solid State Chem. **91**, 140 (1991).
[3] C. B. H. Evers, L. Boonk, and W. Jeitschko, Z. Anorg. Allg. Chem. **620**, 1028 (1994).
[4] M. E. Danebrock, C. B. H. Evers, and W. Jeitschko, J. Phys. Chem. Solids **57**, 381 (1996).
[5] D. T. Morelli and G. P. Meisner, J. Appl. Phys. **77**, 3777 (1995).
[6] G. P. Meisner, D. T. Morelli, S. Hu, J. Yang, and C. Uher, Phys. Rev. Lett. **80**, 3551 (1998).
[7] G. P. Meisner, Physica B & C **108**, 763 (1981).
[8] I. Shirotani, T. Uchiumi, K. Ohno, C. Sekine, Y. Nakazawa, K. Kanoda, S. Todo, and T. Yagi, Phys. Rev. B **56**, 7866 (1997).
[9] E. D. Bauer, N. A. Frederick, P.-C. Ho, V. S. Zapf, and M. B. Maple, Phys. Rev. B **65**, 100506(R) (2002).
[10] G. A. Slack, in *CRC Handbook of Thermoelectrics*, edited by D. M. Rowe (Chemical Rubber, Boca Raton, 1995), p. 407.
[11] I. Oftedal, Z. Kristallogr. **A66**, 517 (1928).
[12] V. Keppens, D. Mandrus, B. C. Sales, B. C. Chakoumakos, P. Dai, R. Coldea, M. B. Maple, D. A. Gajewski, E. J. Freeman, and S. Bennington, Nature (London) **395**, 876 (1998).
[13] R. P. Hermann, R. Jin, W. Schweika, F. Grandjean, D. Mandrus, B. C. Sales, and G. Long, Phys. Rev. Lett. **90**, 135505 (2003).
[14] B. C. Sales, MRS Bull. **23**, 15 (1998).
[15] B. Sales, B. Chakoumakos, and D. Mandrus, Phys. Rev. B **61**, 2475 (2000).
[16] D. Cao, F. Bridges, S. Bushart, E. D. Bauer, and M. B. Maple, Phys. Rev. B **67**, 180511(R) (2003).
[17] J. L. Feldman, D. J. Singh, C. Kendziiora, D. Mandrus, and B. C. Sales, Phys. Rev. B **68**, 094301 (2003).
[18] J. J. Rehr, C. H. Booth, F. Bridges, and S. I. Zabinsky, Phys. Rev. B **49**, 12347 (1994).
[19] S. I. Zabinsky, J. J. Rehr, A. Ankudinov, R. C. Albers, and M. J. Eller, Phys. Rev. B **52**, 2995 (1995).
[20] T. M. Hayes and J. B. Boyce, in *Solid State Physics* (Academic, New York, 1982), Vol. 37, p. 173.
[21] F. Bridges, C. H. Booth, and G. G. Li, Physica B **208–209**, 121 (1995).
[22] G. G. Li, F. Bridges, and C. H. Booth, Phys. Rev. B **52**, 6332 (1995).
[23] Please go to website (http://lise.lbl.gov) for *r*-space EXAFS data analysis package.
[24] E. A. Stern, Phys. Rev. B **48**, 9825 (1993).
[25] B. K. Teo, *EXAFS: Basic Principles and Data Analysis* (Springer-Verlag, New York, 1986).
[26] J. L. Feldman, D. J. Singh, I. I. Mazin, D. Mandrus, and B. C. Sales, Phys. Rev. B **61**, R9209 (2000).
[27] F. Bridges, CRC Crit. Rev. Solid State Sci. **5**, 1 (1975).
[28] F. Bridges and D. Chow, Phys. Rev. Lett. **54**, 1532 (1985).
[29] B. Sales, B. Chakoumakos, R. Jin, J. Thompson, and D. Mandrus, Phys. Rev. B **63**, 245113 (2001).
[30] F. Bridges, R. Baumbach, D. Cao, P. Chesler, M. Anderson, and B. Sales, Radiat. Eff. Defects Solids **158**, 343 (2003).

[31] Z. Kvitky, F. Bridges, and G. van Dorssen, Phys. Rev. B **64**, 214108 (2001).
[32] B. C. Sales, B. C. Chakoumakos, D. Mandrus, and J. Sharp, in *18th Intr. Conf. Thermoelectrics* (IEEE, (Cat. No.99TH8407), Piscataway, NJ, 1999), pp. 525–530.
[33] S. V. Dordevic, N. R. Dilley, E. D. Bauer, N. D. Basov, and M. B. Maple, Phys. Rev. B **60**, 11321 (1999).
[34] T. Caillet, J.-P. Fleurial, and A. Borshchevsky, J. Cryst. Growth **166**, 722 (1996).
[35] G. A. Slack and V. Tsoukala, J. Appl. Phys. **77**, 3777 (1995).
[36] G. J. Long, D. Hautot, F. Grandjean, D. T. Morelli, and G. P. Meisner, Phys. Rev. B **60**, 7410 (1999).
[37] E. Bauer, A. Galatanu, H. Michor, G. Hilscher, P. Rogl, P. Boulet, and H. Noël, Eur. Phys. J. B **14**, 483 (2000).
[38] N. R. Dilley, E. J. Freeman, E. D. Bauer, and M. B. Maple, Phys. Rev. B **58**, 6287 (1998).
[39] C. Sekine, K. Akita, N. Yanase, I. Shirotani, I. Inagawa, and C.-H. Lee, Jpn. J. Appl. Phys., Part 1 **40**, 3326 (2001).